

Structures of an electrorheological fluid

G. L. Gulley and R. Tao

Department of Physics, Southern Illinois University at Carbondale, Carbondale, Illinois 62901-4401

(Received 11 October 1996)

Extensive computer simulations were carried out to examine the structures of electrorheological (ER) fluids. In a weak electric field, ER fluids move from a liquid state to a nematic-liquid-crystal state that has ordering only in the field direction. If the electric field is strong and thermal fluctuations are weak or moderate, ER fluids develop into a body-centered-tetragonal lattice. A very strong electric field with very weak or no thermal fluctuations may force ER fluids into a polycrystalline structure. When both the electric field and thermal fluctuation are strong, ER fluids develop into a glasslike state, in which the particles aggregate together to form thick columns, but the structure has no appreciable ordering. The simulation has also shown that the solidification time and chain formation time in ER fluid systems depend mainly on the ratio of the viscous force to the dipolar force. [S1063-651X(97)02509-9]

PACS number(s): 83.20.Jp, 83.80.Gv, 61.90.+d

I. INTRODUCTION

Electrorheological (ER) fluids are a class of materials whose rheological characteristics are controllable through the application of an electric field. A typical ER fluid consists of colloidal dispersions of dielectric particles in a liquid of low dielectric constant. When an electric field is applied, the effective viscosity of the ER fluid increases dramatically. If the field exceeds a critical value, the ER fluid turns into a solid whose shear stress continues to increase as the field is further strengthened [1–5].

It is known that, upon application of an electric field, the dielectric particles in ER fluids form chains spanning the electrodes. The chains can go on to form thick columns [6]. The body-centered-tetragonal lattice was predicted theoretically as the ground-state structure for an ER fluid and has been verified experimentally [4,7]. The microstructure of ER fluids is a fundamental issue. The mechanical and physical properties of ER fluids depend strongly on the induced structure. For example, the thick-column structure has a higher shear stress than the single-chain structure [8]. Recently, the ER effect has also been used to produce new composite materials [9,10]. Therefore, information about the microstructure of ER fluids under various conditions is very important for the growing number of applications.

In this paper, we will apply a molecular-dynamics simulation to investigate the structure. Our ER system is confined between two electrodes located at $z=0$ and $z=L$, respectively, upon which a voltage may be applied. The system consists of spherical dielectric particles of diameter σ and dielectric constant ϵ_p suspended in a nonconducting liquid. The liquid has a dielectric constant of ϵ_f and viscosity η . In an electric field, each particle has an induced dipole moment of $\mathbf{p} = \alpha \epsilon_f (\sigma/2)^3 \mathbf{E}_{loc}$, where $\alpha = (\epsilon_p - \epsilon_f) / (\epsilon_p + 2\epsilon_f)$ and \mathbf{E}_{loc} is the local field. The formation of structure is driven by dipolar interactions, viscous drag forces, and Brownian motions. Molecular simulations on this model have shown that the ER fluid can readily form the bct lattice under a strong electric field [11]. Several other computer simulations on a similar model have also been reported [12–16]. Some groups also found a crystalline structure [13,16], but some did not

[14]. In order to clarify the issue and understand the detail of the induced structure under various conditions, we carried out extensive computer simulations.

Our results indicate that ER fluids under an electric field may develop into five different structures under different conditions. In a weak electric field, ER fluids can move from a liquid state to a nematic-liquid-crystal state which only has ordering in the field direction, but no ordering in other directions [17]. This ordering indicates chain formation along the field direction. In both liquid and liquid-crystal states, the columnar particle density remains uniform. When the electric field is strong and the thermal fluctuation is weak or moderate, ER fluids develop into a body-centered-tetragonal (bct) lattice. In a very strong field with or without very weak thermal fluctuations, ER fluids may develop into a polycrystalline structure consisting of many small bct lattice grains. If both the electric field and thermal fluctuation are strong, ER fluids develop into a glasslike structure in which the particles are aggregated together to form thick columns, but the structure has no appreciable ordering. In all of the last three structures, the columnar particle density peaks in a small region, indicating a thick-column structure.

Our simulation also provides information about the solidification and the chain formation time in ER fluids. The chain formation time is much shorter than the solidification time. Both of them depend mainly on the ratio of the viscous force to the dipolar force, especially in the overdamped case. However, when the viscosity is not too strong, the ratio of the Brownian force to the dipolar force also plays a role in these two time scales.

II. SIMULATION

We use the Langevin equation to describe the motion of particle i :

$$m \frac{d^2 \mathbf{r}_i}{dt^2} = \mathbf{F}_i - 3\pi\sigma\eta \frac{d\mathbf{r}_i}{dt} + \mathbf{R}_i(t). \quad (1)$$

Here \mathbf{F}_i includes all electric forces on particle i , $3\pi\sigma\eta\mathbf{v}_i$ is the Stokes' drag force, and $\mathbf{R}_i(t)$ is a Brownian force. \mathbf{F}_i is given by the expression

$$\mathbf{F}_i = \sum_{j \neq i} [\mathbf{f}_{ij} + \mathbf{f}_{ij}^{\text{rep}}] + \mathbf{f}_i^{\text{self}} + \mathbf{f}_i^{\text{wall}}, \quad (2)$$

where \mathbf{f}_{ij} is the force acting on particle i by particle j and all of j 's images, $\mathbf{f}_{ij}^{\text{rep}}$ is a short-range repulsive force to prevent particles i and j from overlapping, $\mathbf{f}_i^{\text{self}}$ is the force on particle i due to all its own images, and $\mathbf{f}_i^{\text{wall}}$ is a short-range repulsive force to prevent particle i from penetrating the two electrodes.

The dipolar force exerted by particle j on particle i is given by

$$\frac{3p^2}{(\epsilon_f r_{ij}^4)} [\mathbf{e}_r(1 - 3 \cos^2 \theta_{ij}) - \mathbf{e}_\theta \sin 2\theta_{ij}], \quad (3)$$

where $\mathbf{r}_{ij} = \mathbf{r}_i - \mathbf{r}_j$, and θ_{ij} is the angle between the z direction and the joint line of the two dipoles. When a dipole is placed inside a capacitor at $\mathbf{r}_i = (x_i, y_i, z_i)$, an infinite number of images are produced at $(x_i, y_i, -z_i)$ and $(x_i, y_i, 2Lk \pm z_i)$ for $k = \pm 1, \pm 2, \dots$. The force that the j th particle and its images exert on the i th particle is given by

$$\begin{aligned} f_{ij,x} &= \frac{p^2}{\epsilon_f L^4} \sum_{s=1}^{\infty} \frac{4s^3 \pi^3 (x_i - x_j)}{\rho_{ij}} K_1 \left(\frac{s\pi \rho_{ij}}{L} \right) \cos \left(\frac{s\pi z_i}{L} \right) \\ &\quad \times \cos \left(\frac{s\pi z_j}{L} \right), \\ f_{ij,y} &= \frac{p^2}{\epsilon_f L^4} \sum_{s=1}^{\infty} \frac{4s^3 \pi^3 (y_i - y_j)}{\rho_{ij}} K_1 \left(\frac{s\pi \rho_{ij}}{L} \right) \cos \left(\frac{s\pi z_i}{L} \right) \\ &\quad \times \cos \left(\frac{s\pi z_j}{L} \right), \\ f_{ij,z} &= \frac{p^2}{\epsilon_f L^4} \sum_{s=1}^{\infty} 4s^3 \pi^3 K_0 \left(\frac{s\pi \rho_{ij}}{L} \right) \sin \left(\frac{s\pi z_i}{L} \right) \cos \left(\frac{s\pi z_j}{L} \right), \end{aligned} \quad (4)$$

where $\rho_{ij} = \sqrt{(x_i - x_j)^2 + (y_i - y_j)^2}$, and K_0 and K_1 are modified Bessel functions.

The force on a particle due to its own images is in the z direction, and given by

$$f_{i,z}^{\text{self}} = \frac{3p^2}{8\epsilon_f} \left[-\frac{1}{z_i^4} + \sum_{s=1}^{\infty} \frac{1}{(z_i - sL)^4} - \frac{1}{(z_i + sL)^4} \right]. \quad (5)$$

To introduce hard spheres and hard walls into the simulation, we use a short-range repulsion between two particles,

$$\mathbf{f}_{ij}^{\text{rep}} = \frac{3p^2 \mathbf{e}_r}{\epsilon_f \sigma^4} \exp[-100(r_{ij}/\sigma - 1)], \quad (6)$$

and the short-range repulsion between a particle and the electrodes as

$$\begin{aligned} \mathbf{f}_i^{\text{wall}} &= \frac{3p^2 \mathbf{e}_z}{\epsilon_f L^4} \{ \exp[-100(z_i/\sigma - 0.5)] \\ &\quad - \exp[-100((L - z_i)/\sigma - 0.5)] \}. \end{aligned} \quad (7)$$

The random force $\mathbf{R}_i(t)$ has a white-noise distribution

$$\langle R_{i,x} \rangle = 0, \quad \langle R_{i,\alpha}(0) R_{i,\beta}(t) \rangle = 6\pi k_B T \sigma \eta \delta_{\alpha\beta} \delta(t), \quad (8)$$

where k_B is Boltzmann's constant, and T is the temperature. We introduce a subinterval τ which is shorter than the time steps used in the integration of Eq. (1), but much longer than the molecular collision time [18]. The average of $\mathbf{R}_i(t)$ over τ , $R_{i,\alpha}(t, \tau) = (1/\tau) \int_t^{t+\tau} R_{i,\alpha}(t') dt'$, has a Gaussian distribution

$$W(R_{i,\alpha}(t, \tau)) = \frac{1}{(2\pi)^{1/2} \Omega} \exp[-(R_{i,\alpha}(t, \tau))^2 / (2\Omega^2)], \quad (9)$$

where $\Omega = \sqrt{6\pi k_B T \sigma \eta / \tau}$. For a time step $\delta t > \tau$, we can divide it into many subintervals of duration τ , in which all quantities except $\mathbf{R}_i(t)$ can be treated as constants. Then, for any smooth function ψ , $X_\alpha = \int_t^{t+\delta t} \psi(\xi) R_{i,\alpha}(\xi) d\xi$ has a probability distribution

$$W(X_\alpha) = (\pi q)^{-1/2} \exp(-X_\alpha^2 / q), \quad (10)$$

where $q = 12\pi k_B T \sigma \eta \int_t^{t+\delta t} \psi^2(\xi) d\xi$, and is independent of τ . Although the value of τ is not very uniquely defined, Eq. (10) implies that our results do not depend on a specific choice of τ .

The intrinsic time scale in Eq. (1) is $t_0 = m / (3\pi\sigma\eta)$. We rescale the variables $t = t_0 t^*$, $\mathbf{F}_i = F_0 \mathbf{F}_i^*$, where $F_0 = 3p^2 / (\epsilon_f \sigma^4)$, $\mathbf{R}_i = \Omega \mathbf{R}_i^*(t)$, and $\mathbf{r}_i = \sigma \mathbf{r}_i^*$ in Eq. (1). The scaling produces a new equation

$$\ddot{\mathbf{r}}_i^* + \dot{\mathbf{r}}_i^* = A(\mathbf{F}_i^* + B\mathbf{R}_i^*), \quad (11)$$

where $A = F_0 t_0 / (3\pi\eta\sigma)$ and $B = \Omega / F_0$. It is interesting to note that A is the ratio of the Reynolds number to the Mason number. The Reynolds number R is the ratio of the inertial force $m v^2 / \sigma$ to the viscous force $3\pi\sigma\eta v$, where v is the speed of dielectric particles. Hence $R = m v / (3\pi\eta\sigma^2) = v t_0 / \sigma$. The Mason number Mn is the ratio of the viscous force to the dipolar force, $Mn = 3\pi\sigma\eta v / F_0$. Then, it is clear that $A = R / Mn$. In our problem, dielectric particles have negligible speed before the electric field is applied or after the solid structure is formed. During the process, the particles have either steady or typical speed. As a result, there is no typical Reynolds number or Mason number in our problem. However, their ratio A is independent of the particle speed, and hence is a good parameter for our simulation.

We also note that parameter B is the ratio of the Brownian force to the dipolar force. In addition, $1/(AB^2) = (1.5\tau/t_0)\lambda$, where $\lambda = (p^2 / \epsilon_f \sigma^3) / k_B T$, a crucial parameter [19] in the study of an ER system in the equilibrium process [17]. However, we must remember that our electric-field-induced solidification is a nonequilibrium process, during which the temperature is not uniform throughout the system.

In our simulation we use 122 particles confined in a cell of dimensions $L_x = L_y = 5\sigma$ and $L_z = 14\sigma$. This corresponds to a volume fraction of $\phi = 0.183$. There are periodic boundary conditions in the x and y directions. We probe the structure at each step using the following three order parameters:

$$\rho_j = \left| \frac{1}{N} \sum_{i=1}^N \exp(i\mathbf{b}_j \cdot \mathbf{r}_i) \right|, \quad (12)$$

where \mathbf{b}_j are the reciprocal-lattice vectors of the bct lattice,

$$\begin{aligned}\mathbf{b}_1 &= (2\pi/\sigma)(2\mathbf{e}'_x/\sqrt{6}-\mathbf{e}_z), \\ \mathbf{b}_2 &= (2\pi/\sigma)(2\mathbf{e}'_y/\sqrt{6}-\mathbf{e}_z), \quad \mathbf{b}_3 = 4\pi\mathbf{e}_z/\sigma.\end{aligned}\quad (13)$$

Of the three unit vectors, \mathbf{e}_z is along the field direction, and \mathbf{e}'_x and \mathbf{e}'_y are along the intrinsic axes of the bct lattice. In the calculation of the order parameters, we must rotate the coordinate system around the z axis to find the intrinsic axes of the structure which maximizes $\rho_1\rho_2$. The order parameter ρ_3 characterizes the structure along the z direction, while ρ_1 and ρ_2 characterize structure in the x - y plane.

In the simulation, we assume that an electric field is applied at $t=0$ instantaneously. Then we apply an adaptive step-size control Runge-Kutta method to integrate the equation of motion. It is clear from Eq. (11) that the final structure depends on the two parameters A and B . We examine the dynamic process by monitoring the particles' positions, velocities, and the structure's order parameters. In most cases, after application of the field, the particles quickly move to form chains, then the chains aggregate to form a thick structure. Afterwards, the particles usually fluctuate slightly around their positions in the structure, and the order parameters of the system change very little. Hence we are able to determine the solidification time and analyze the final structure. The other interesting quantity is the chain formation time which is shorter than the solidification time.

As seen from Eqs. (6) and (7), collisions may interrupt the structure formation if some particle's position change in the integration is too large. Therefore, we specify a value δr_c . If the largest position change among all the particles' motion during one time step δt is greater than δr_c , the next time step is reduced. Otherwise, δt will be increased. Our method speeds up the integration and effectively prevents possible problems from the collisions, because we control the position change by selecting a proper δr_c . Since the time step changes at every step with this method, we must employ Eq. (10) to handle the Brownian force.

There are some special situations which need to be discussed. In the overdamped case, the viscous force becomes so strong that we have

$$\ddot{\mathbf{r}}_i^* = -\dot{\mathbf{r}}_i^* + A(\mathbf{F}_i^* + B\mathbf{R}_i^*) \approx 0. \quad (14)$$

The overdamping condition requires

$$|A(\mathbf{F}_i^* + B\mathbf{R}_i^*)| \ll 1. \quad (15)$$

Equation (11) can then be simplified to

$$\dot{\mathbf{r}}_i^* = A(\mathbf{F}_i^* + B\mathbf{R}_i^*). \quad (16)$$

Now, setting $t^* = \zeta/A$, we have

$$d\mathbf{r}_i^*/d\zeta = \mathbf{F}_i^* + B\mathbf{R}_i^*, \quad (17)$$

which is independent of A . Therefore, in the overdamped case the final structure is independent of A , but the solidification time is inversely proportional to A . From Eq. (15), $A \ll 1/(F_{\max}^* + B)$ is required to see the overdamped case. The maximum force F_{\max}^* comes when there are collisions be-

tween the particles or collisions between the particles and the electrodes. In our simulation, we have found that when $A \leq 10^{-3}$, the final structure has its three order parameters independent of A and the solidification time is proportional to $1/A$, indicating that the system is in the overdamped situation.

The effect of the random force BR^* in Eq. (11) needs special attention. Since R_i^* is a Gaussian deviate, we should compare the magnitude of F_i^* with B . When the particles are randomly distributed in the cell, the typical value of F_i^* in Eq. (11) is $\sim n^{4/3}$, where n is the particle density. In our simulation $n=0.3486$, which gives an estimation of 0.2 for the typical value of F_i^* for a random distribution. When two particles come very close, their dipolar interaction force has a typical value ~ 1 . However, when the particles aggregate to form a final structure, the joint forces on every particle are vanishingly small. Therefore, it is easy to understand from Eq. (11) that if $B \ll 0.2$, BR_i^* has little effect on the early dynamic process, but may have some effect on the final structure since the joint forces on each particle are small. If $B \gg 1$, BR_i^* becomes the leading force in Eq. (11).

III. STRUCTURES

If the ER system can always evolve into its equilibrium state after an electric field is applied, the final structure may only depend on the parameter $\lambda = p^2/(\epsilon_f \sigma^3 k_B T)$. However, in the actual dynamic process, the ER system may not be able to reach the ground state after it is trapped in a local-energy minimum state. The viscous force enhances such a possibility by a quick reduction of the particles' kinetic energy.

In order to make a comparison, we derive all these final structures in our simulation from an initial randomly distributed state (Fig. 1). As we vary the two parameters A and B , we clearly see five different structures of ER fluids: liquid structure, nematic-liquid-crystal structure, glasslike structure, polycrystalline structure, and bct lattice structure. Figure 2 depicts the final structures the system evolves into over a wide range of A and B . In Fig. 2(a), we present the result with axes A and B . In Fig. 2(b), we present the same result with axes A and λ . The boundary between the liquid and the nematic liquid crystal and the boundary between the bct lattice structure and the nematic-liquid-crystal structure seem to have $\lambda=6.7$ and 167 respectively. Although this is expected for equilibrium statistical physics, we should note that the final structure in our simulation may not be the equilibrium state. Therefore, Fig. 2 may differ from a conventional phase diagram.

A. bct lattice and polycrystalline structure

As seen from Fig. 2, the ordered state, a bct lattice, has been obtained in quite a wide range of A and B . In Fig. 3, we plot a typical bct lattice structure with order parameters $\rho_1, \rho_2 \approx 0.8$ and $\rho_3 \geq 0.9$. The projection of the three-dimensional structure onto the x - y plane shows a centered square lattice (Fig. 4), a typical characterization of the bct lattice [4], the marked square also has its side $\sim \sqrt{1.5}\sigma$, and the characterization of these chains is also correct for the bct lattice [4].

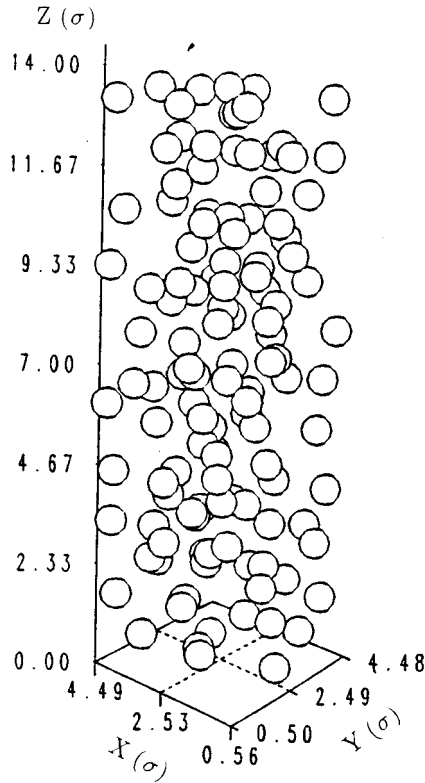


FIG. 1. The initial state has the particles randomly distributed in space.

We also note that there is a small region inside this ordered region where the system may likely develop into a polycrystalline structure (Fig. 5). This small region has a very small B and a large A (≥ 0.1). Examination of this structure reveals that the system has thick columns consisting of several bct lattice grains. However, these grains do not form a single crystal. There is some mismatch, mainly caused by their rotation around the z axis by slightly different angles. In Fig. 6, we plot a part of a thick column of polycrystalline structure which clearly shows a twist of bct lattice grains. Since these rotations do not affect ρ_3 very much but reduces ρ_1 and ρ_2 , ρ_3 remains ~ 0.9 , while ρ_1 and ρ_2 are reduced to ~ 0.5 . The polycrystalline structure is a product of fast solidification. Because of a very small B in this region, the ER system may not be able to relax into a good crystal. It is thus easy to understand that in this region the final structure is somehow sensitive to the initial random state. The computer simulation confirms this conclusion too: in this region from some random initial state the ER system may develop into a good bct lattice, while from some other random initial state the system ends up in a polycrystalline structure.

To further understand the issue, we paid special attention to the situation of $B=0$ which can be realized at zero temperature. If $A \leq 10^{-3}$, the system is overdamped. The final structure has three order parameters independent of A : ρ_1 and ρ_2 around 0.62, and ρ_3 around 0.89. If A is between 10^{-3} and 0.1 with $B=0$, the final structure is improved with ρ_1 and ρ_2 around 0.8–0.9, and ρ_3 around 0.90–0.93, a rather good bct lattice. The order parameters of the final structure in this region depends on A . As A continues to increase, the

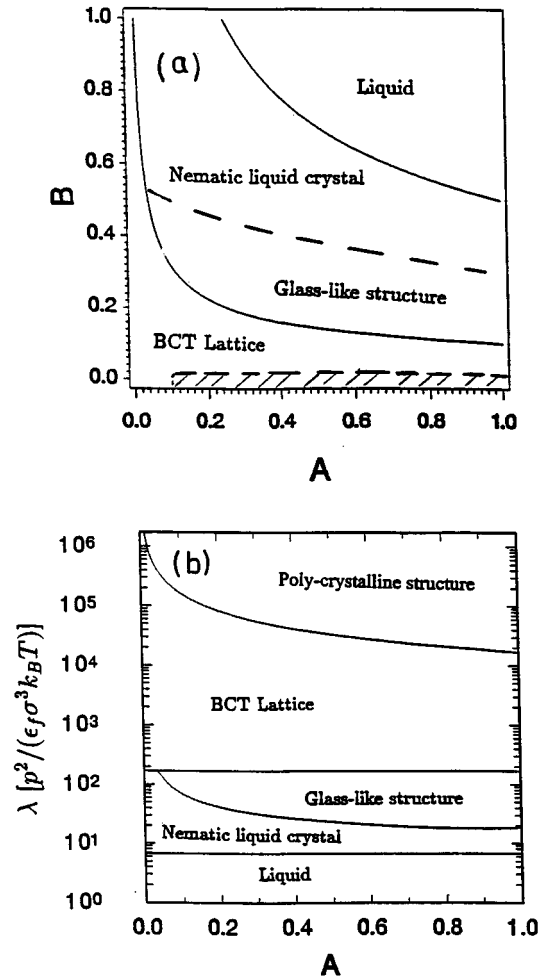


FIG. 2. (a) Different structures under various conditions. In the shaded area, ER fluids may develop into a polycrystalline structure. The boundary between the liquid and the nematic liquid crystal has $AB^2 \sim 0.25$ ($\lambda \sim 6.7$). The boundary between the bct lattice and liquid crystal state has $AB^2 \sim 10^{-2}$ ($\lambda \sim 167$). (b) The same results presented with axes A and λ . The polycrystalline structure and glasslike structure are nonequilibrium products.

three order parameters are fluctuating in the polycrystalline region. For example, when $A \geq 0.1$ and $B=0$, the final structure developed from the initial state in Fig. 1 has three order parameters around 0.5, while ρ_3 is close to 0.6. However, the final structure at $A \geq 0.1$ and $B=0$ is now very sensitive to the initial random state. For example, after changing the initial state at $A=0.1$ and $B=0$, we ended up with a good bct lattice: ρ_1 and ρ_2 are close to 0.84, and ρ_3 is close to 0.92. This also implies that the ER system at $B=0$ can be easily trapped in a local-energy minimum. The final structures derived at a moderate B are not sensitive to the initial random state because the ER system can obtain from a local minimum-energy state and develop into the global energy-minimum state with the help of the thermal fluctuations.

We also compared the final structures in the polycrystalline region when we fix A and increase B . For example, at $A=1.0$ and $B=0$, the final structure derived from the initial state in Fig. 1 has ρ_1 and ρ_2 around 0.5–0.6, and ρ_3 about 0.83. When we increase B , although we continue to start the system from the same initial state, the final structure im-

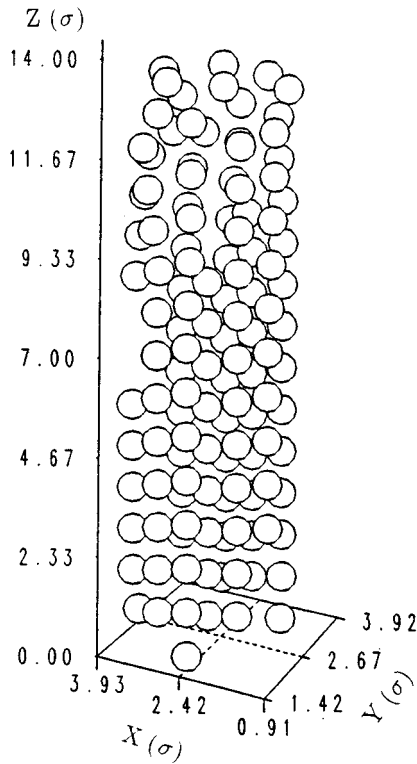


FIG. 3. A good body-centered-tetragonal lattice is formed with $\rho_1, \rho_2 \approx 0.8$ and $\rho_3 \geq 0.9$.

proves. For example at $A = 1.0$ and $B = 0.1$, the final structure has ρ_1 and ρ_2 around 0.8 and ρ_3 around 0.87. This implies that a moderate B can help the system relax into a global energy minimum state.

B. Nematic-liquid-crystal and glasslike structures

When we increase B , equivalent to raising the temperature, we come from the region of the bct lattice to a region of final structure with significant ρ_3 , but small ρ_1 and ρ_2 . Typically, ρ_1 and ρ_2 are around 0.3 while $\rho_3 \geq 0.6$. This

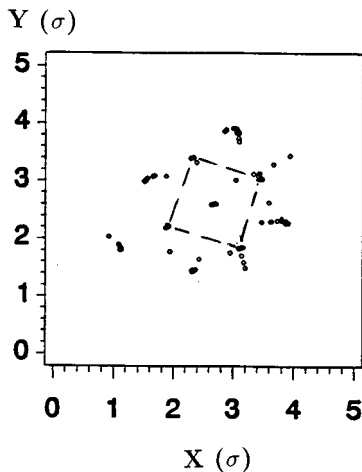


FIG. 4. Projection of the bct lattice on the $x-y$ plane. The marked square has its side $\sim \sqrt{1.5}\sigma$.

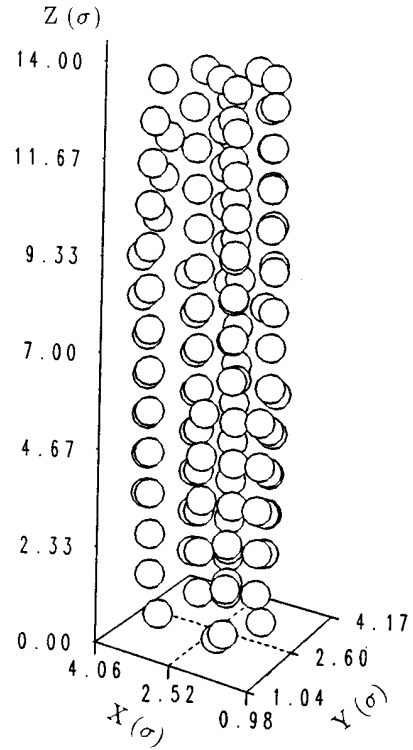


FIG. 5. A polycrystalline structure.

implies that the system has ordering in the z direction with weak or no ordering in the $x-y$ directions. From the definition of a particle density

$$D(\mathbf{r}) = \sum_{j=1}^N \delta(\mathbf{r} - \mathbf{r}_j), \tag{18}$$

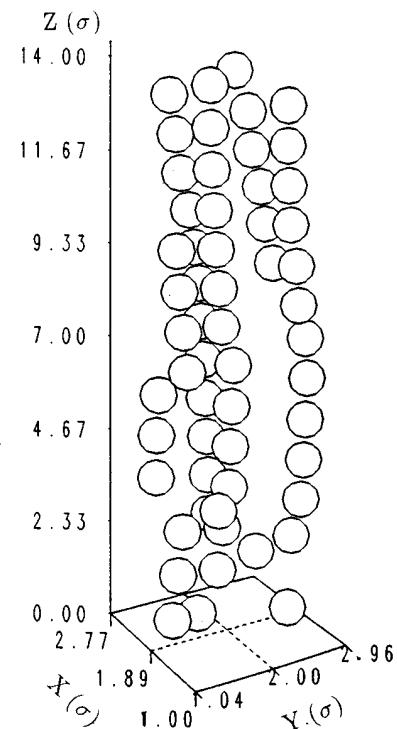


FIG. 6. A thick column of polycrystalline structure which clearly shows a twist of bct lattice grains.

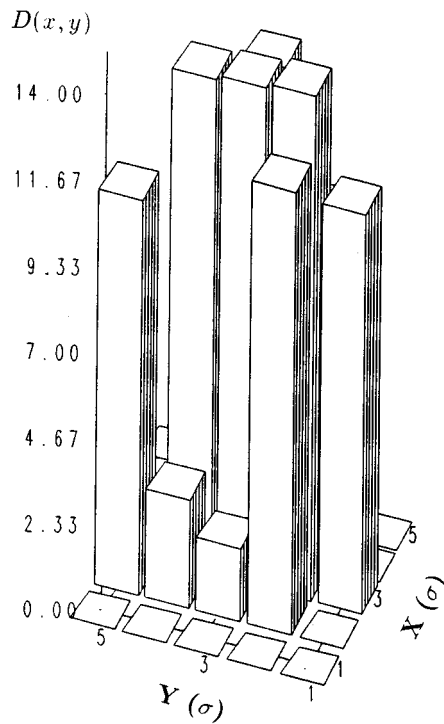


FIG. 7. In a nematic-liquid-crystal state, the particles do not aggregate together. $D(x,y)$ is quite uniform over most of the region.

where \mathbf{r}_j is the position of the j th particle center, we define a columnar density,

$$D(x,y) = \int_0^L D(\mathbf{r}) dz. \quad (19)$$

After analyzing the columnar density of these structures, we find that, within this region, there are two slightly different structures. When A is relatively small and B is relatively strong, $D(x,y)$ is quite uniform, as in Fig. 7. This implies that, in these structures, the particles do not aggregate together to form thick columns, though there is some ordering in the field direction. The system remains in a liquid state, but similar to a nematic-liquid-crystal structure (Fig. 8). When A is relatively strong and B is relatively small, the ER fluids form thick columns. As indicated by $D(x,y)$ in Fig. 9, the particles are concentrated in a small region, a main difference distinguishing this structure from a nematic-liquid-crystal structure. The three order parameters of this structure are not too much different from that of a nematic-liquid-crystal structure. Although there is some ordering in the field direction, there is no significant lateral ordering. Therefore, this is a glasslike structure (Fig. 10). In this region, the strong electric field forces the particles to aggregate to form thick columns, but the thermal fluctuations prevent the system from forming a crystalline structure.

C. Liquid

A further increase of B leads to a region which has the final structure in a liquid state (Fig. 11). All three order pa-

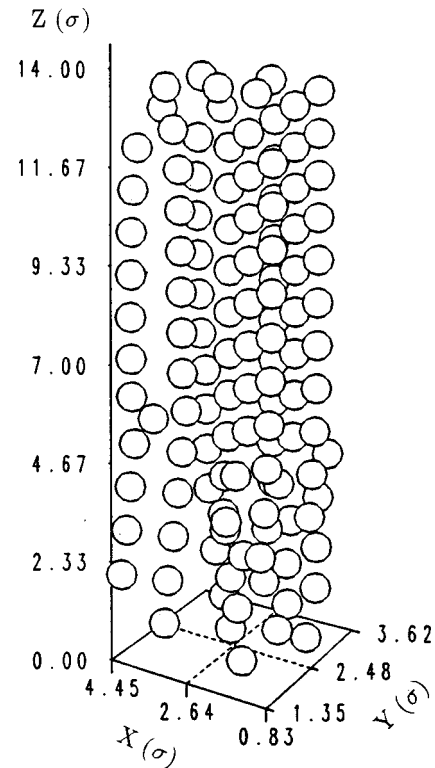


FIG. 8. In a nematic-liquid-crystal state, the system has ordering in the z direction but almost no ordering in the $x-y$ directions.

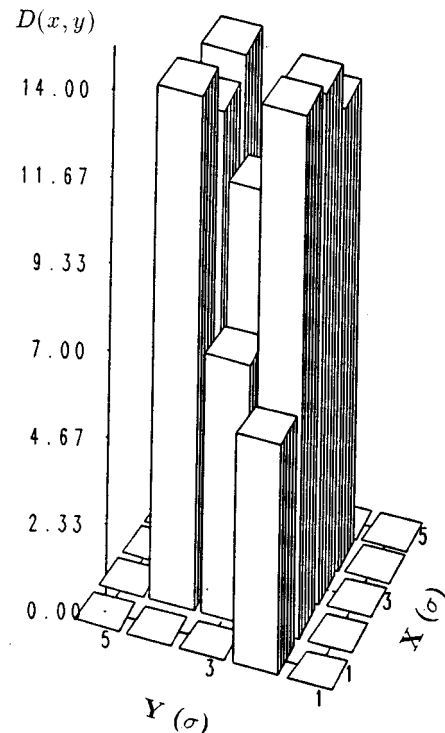


FIG. 9. In a glasslike structure, $D(x,y)$ is peaked in a small columnar region, a main difference between a glasslike structure and liquid.

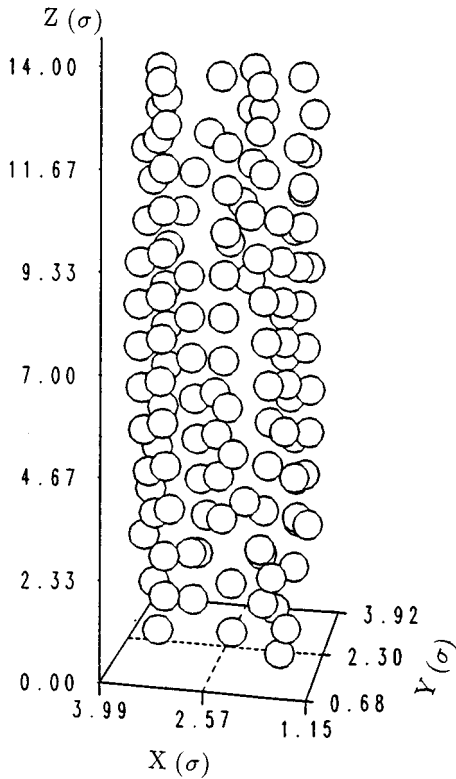


FIG. 10. In a glasslike structure, the ER fluids form thick columns, but the three order parameters are almost the same as that of the nematic-liquid-crystal state.

rameters are very small for these structures. The particles are randomly and quite uniformly distributed in the space, as seen from $D(x,y)$ in Fig. 12. In this region, the random Brownian force is too strong to prevent formation of any ordered structures.

D. Nonequilibrium process and boundaries

Our simulation shows a dynamic process. The polycrystalline structure is a product of nonequilibrium processes. The difference between the glasslike structure and liquid crystal is only in the columnar density, not in the ordering. In a glasslike structure, the particles aggregate together while they do not in a nematic liquid crystal (see Figs. 7 and 9). Therefore, polycrystalline and glasslike structures may not be closely related to the equilibrium state. On the other hand, both the boundaries between the liquid and nematic-liquid-crystal structures and the bct lattice and liquid-crystal structures seem to be related to the equilibrium state. Although they are not exact, these two boundaries both have AB^2 roughly as a constant. Since the parameter λ is proportional to $1/(AB^2)$, these two boundaries are roughly along the lines of a constant λ [17]. The boundary between the liquid and the nematic liquid crystal has AB^2 close to 0.25, corresponding to $\lambda \sim 6.7$. The boundary between the bct lattice and liquid-crystal state has AB^2 close to 10^{-2} , corresponding to $\lambda \sim 167$.

IV. SOLIDIFICATION TIME

ER fluids are marked for their fast response to an electric field. A number of experiments established that a typical

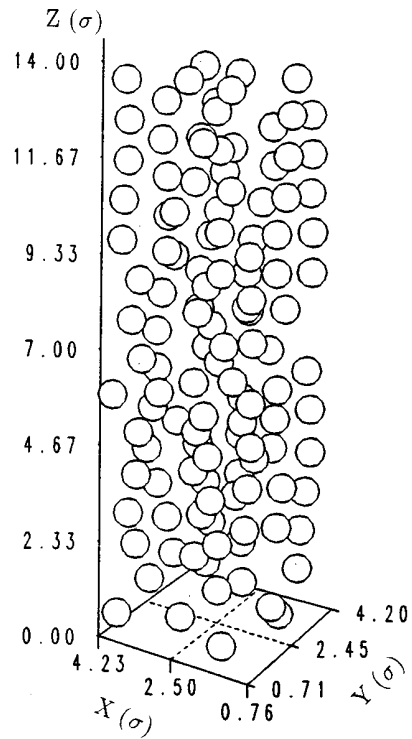


FIG. 11. In a liquid state, three order parameters are vanishingly small, and the particles are randomly distributed in the space.

response time of ER fluids is of the order of milliseconds. This response time is usually defined as the time needed for ER fluids to have a significant viscosity increase immediately after an electric field is applied. In our simulation, we define the solidification time as the time interval between the application of an electric field and the establishment of a final structure [20]. It is clear that our solidification time should be longer than the response time since ER fluids deliver a significant increase of viscosity before they reach their final structure. However, these two time scales are closely related, and our solidification time has clear physical meaning and is important for applications as well.

The relationship between the solidification time and the parameters A and B is in Fig. 13. We note that, at a fixed B , the solidification time grows longer as A becomes smaller. In the overdamped case, Eq. (17) indicates that the solidification time is inversely proportional to A . Our simulation verifies this conclusion: the solidification time in the overdamped case goes as

$$t_{\text{solid}} = 60/A. \quad (20)$$

This relationship holds up to $A \sim 10^{-2}$. In real time, for example, at $A = 10^{-3}$, this solidification time is of the order of a second. As the value of A increases, the viscosity reduces. When the system is not overdamped, the solidification time further decreases as A increases, but this reduction is slower than $1/A$. For example, as A increases from 10^{-2} to 10^{-1} , the solidification time only slightly reduces.

At a fixed A , the solidification time increases with B . This is due to high fluctuations of the Brownian motion. However, the effect of B is significant only when B is large enough. For example, if $B < 10^{-2}$, the solidification time is

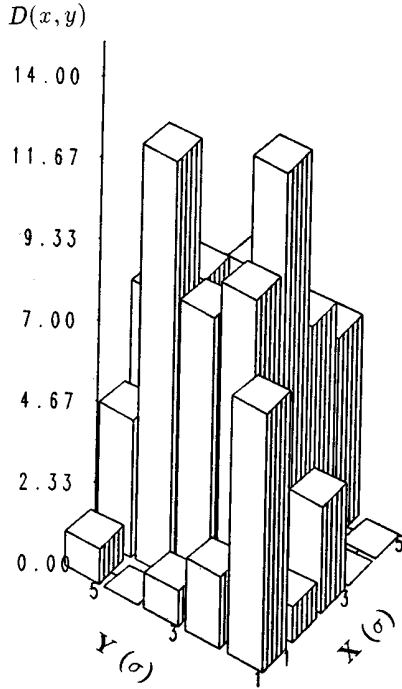


FIG. 12. In the liquid state, $D(x,y)$ is quite uniform over the whole region.

almost unaffected by B . If $B > 10^{-2}$, the thermal fluctuations delay the solidification process. For example, at $A = 10^{-3}$ and $B = 10^{-2}$, the formation of a bct lattice structure takes about $1.738 \times 10^5 t_0$, while at $A = 10^{-3}$ and $B = 10^{-1}$ the solidification of a similar bct lattice takes $2.81 \times 10^5 t_0$.

In our simulation, we also determine the chain formation time by examining the order parameter ρ_3 . From Fig. 14, it is clear that the chain formation is much faster than the formation of a final structure. This again implies that the particles in ER fluids form chains first, then chains aggregate together to form thick columns. Typically, the chain forma-

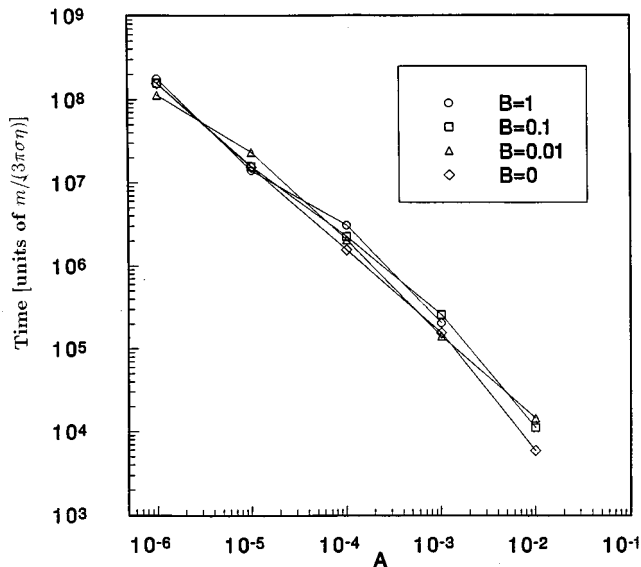


FIG. 13. The relationship between the solidification time and the parameters A and B .

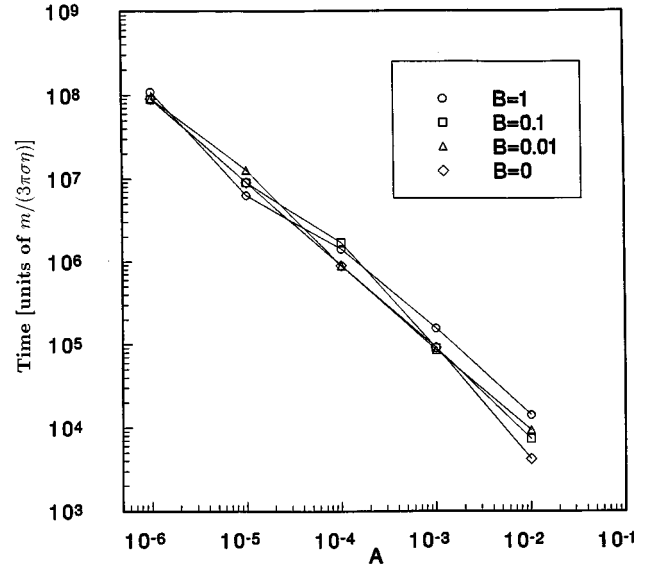


FIG. 14. The relationship between the chain formation time and the parameters A and B .

tion time is about one-third of the solidification time or shorter. In the overdamping case, the chain formation time is also proportional to $1/A$. We also notice that, in real time, the chain formation time is of the order of milliseconds, the same order as the response time found in engineering applications.

V. DISCUSSIONS

In this section, we want to compare our simulation results with experiments. For a real ER system, such as dielectric particles in petroleum oil, $\epsilon_f \sim 2$, $\epsilon_p \gg 1$, $\eta \sim 0.2$ P, $\sigma \sim 10 \mu\text{m}$, and the mass density of the particle $\rho \sim 3 \text{ g/cm}^3$. We estimate $t_0 \sim 8.33 \times 10^{-7}$ s. If we choose the subinterval $\tau = 0.4t_0$, then as E_0 varies from 0 to 4 KV/mm at $T = 300$ K, A changes from 0 to 10^{-2} and B reduces from ∞ to 10^{-3} . When $A = 10^{-2}$ and $B = 10^{-2}$, for example, our simulation finds the chain formation time is about 4 ms, while the bct lattice and the solidification time is less than 1 s. In the experiment, the chain formation takes milliseconds to complete, but the formation of the bct lattice is slower than that in our computer simulation [7].

As the particle size becomes larger the inertial time t_0 and A increase. For example, if the above ER fluid has everything the same except $\sigma \sim 100 \mu\text{m}$ instead of $10 \mu\text{m}$, then we have $A \sim 1$ at $E = 4$ kV/mm. Hence, from Fig. 2, we notice that ER fluids with large particles are easy to develop into a polycrystalline structure in the nonequilibrium process. This interesting result is useful in production of composite materials by the ER effect [9,10].

Our results at $B = 0$ are interesting enough to warrant some experimental investigation. The fact that the final structure at $B = 0$ is sensitive to the initial state indicates that the Brownian force plays an important role in driving the ER system from a local-energy-minimum state into a global energy-minimum state. On the other hand, if B is too strong, the thermal fluctuations prevent the system from forming a good bct lattice. Therefore, an experimental determination of

this range of B will be very interesting. This goal may be achieved by examination of ER fluids at cryogenic temperatures.

Our simulation also reveals that the response time defined in ER engineering applications is related to the chain formation time. We also found a relationship between the solidification time and the viscosity, temperature, and electric field.

It will be very interesting to see if this relationship holds in experiments.

ACKNOWLEDGMENT

This research was supported by National Science Foundation Grant No. DMR-9622525.

-
- [1] For example, see, *Electrorheological Fluids*, edited by R. Tao and G. D. Roy (World Scientific, Singapore, 1994).
- [2] L. C. Davis, *J. Appl. Phys.* **72**, 1334 (1992); **73**, 680 (1993); H. Block and J. P. Kelly, US Patent No. 4,687,589 (18 Aug. 1987).
- [3] F. E. Filisko and W. E. Armstrong, US Patent No. 4,744,914 (17 May 1988).
- [4] R. Tao and J. M. Sun, *Phys. Rev. Lett.* **67**, 398 (1991) *Phys. Rev. A* **44**, R6181 (1991).
- [5] J. E. Martin, J. Odinek, and T. C. Halsey, *Phys. Rev. Lett.* **69**, 1524 (1992).
- [6] R. Tao, J. T. Woestman, and N. K. Jaggi, *Appl. Phys. Lett.* **55**, 1844 (1989).
- [7] T. J. Chen, R. N. Zitter, and R. Tao, *Phys. Rev. Lett.* **68**, 2555 (1992).
- [8] G. L. Gulley and R. Tao, *Phys. Rev. E* **48**, 2744 (1993).
- [9] X. Wy. X. Zhang, R. Tao, and R. P. Reitz, *Bull. Am. Phys. Soc.* **41**, 191 (1996).
- [10] C. A. Randal, C. P. Bowen, T. R. Shrout, G. L. Messing, and R. E. Newnham, in *Electrorheological Fluids* (Ref. [1]), p. 516.
- [11] R. Tao and Q. Jiang, *Phys. Rev. Lett.* **73**, 205 (1994).
- [12] D. J. Klingenberg, F. van Swol, and C. F. Zukoski, *J. Chem. Phys.* **91**, 7888 (1989); **94**, 6170 (1991).
- [13] N. K. Jaggi, *J. Stat. Phys.* **64**, 1093 (1991); W. Toor, *J. Colloid Interface Sci.* **156**, 335 (1993).
- [14] K. C. Hass, *Phys. Rev. E* **47**, 3362 (1993).
- [15] R. T. Bonnecaze and J. F. Brady, *J. Chem. Phys.* **96**, 2183 (1992).
- [16] H. X. Guo, Z. H. Mai, and H. H. Tian, *Phys. Rev. E* **53**, 3823 (1996).
- [17] R. Tao, *Phys. Rev. E* **47**, 423 (1993).
- [18] For example, see S. Chandrasekhar, *Rev. Mod. Phys.* **15**, 1 (1943); R. Reif, *Fundamental of Statistical and Thermal Physics* (McGraw-Hill, New York, 1965), pp. 560–562.
- [19] P. M. Adraini and A. P. Gast, *Phys. Fluids* **31**, 2757 (1988).
- [20] H. See and M. Doi, *J. Phys. Soc. Jpn.* **60**, 2278 (1991).